LETTERS

Magma heating by decompression-driven crystallization beneath andesite volcanoes

Jon Blundy[1], Kathy Cashman[2] & Madeleine Humphreys[1]

Explosive volcanic eruptions are driven by exsolution of H_2O-rich vapour from silicic magma[1]. Eruption dynamics involve a complex interplay between nucleation and growth of vapour bubbles and crystallization, generating highly nonlinear variation in the physical properties of magma as it ascends beneath a volcano[2]. This makes explosive volcanism difficult to model and, ultimately, to predict. A key unknown is the temperature variation in magma rising through the sub-volcanic system, as it loses gas and crystallizes *en route*[3]. Thermodynamic modelling of magma that degasses, but does not crystallize, indicates that both cooling and heating are possible[4]. Hitherto it has not been possible to evaluate such alternatives because of the difficulty of tracking temperature variations in moving magma several kilometres below the surface. Here we extend recent work on glassy melt inclusions trapped in plagioclase crystals[5] to develop a method for tracking pressure–temperature–crystallinity paths in magma beneath two active andesite volcanoes. We use dissolved H_2O in melt inclusions to constrain the pressure of H_2O at the time an inclusion became sealed, incompatible trace element concentrations to calculate the corresponding magma crystallinity and plagioclase–melt geothermometry to determine the temperature. These data are allied to ilmenite–magnetite geothermometry to show that the temperature of ascending magma increases by up to 100 °C, owing to the release of latent heat of crystallization. This heating can account for several common textural features of andesitic magmas, which might otherwise be erroneously attributed to pre-eruptive magma mixing.

Plagioclase-hosted melt inclusions from the 1980–86 eruption of Mount St Helens (Washington, USA) and the 2001–04 eruption of Shiveluch (Kamchatka, Russia) display a wide variety of shapes and textures (Fig. 1). The vast majority of inclusions are glassy rhyolites without daughter microlite crystals. There is compelling chemical and textural evidence[5] that, subsequent to their entrapment, melt inclusions maintained some physical connectivity with the matrix melt, such that melt inclusions and matrix melt evolve in chemical harmony up until the point that the inclusions become physically isolated from the matrix. The predominant crystallizing phase at both volcanoes is plagioclase. Consequently, all inclusions show some evidence of precipitation of this mineral around their walls (Fig. 1c, d). In some cases, plagioclase precipitation proceeds to the extent that the inclusion is almost completely filled-in, leading to a pseudomorphic texture (Fig. 1c).

For those inclusions that have not been completely infilled, the relationship between the chemistry of the inclusion glass and the composition of the immediately adjacent plagioclase in-fill (for example, Fig. 1d) contains information about magmatic conditions at the point of chemical isolation. This is either the point at which the connection between inclusion and matrix became occluded by plagioclase growth, or that at which chemical diffusion along the connection ceased to be viable on the relevant timescale. In essence, chemical equilibrium between inclusion and plagioclase provides a 'snapshot' of the overall ascent path of the magma in which the crystal is found[5]. We analysed 99 melt inclusions and their adjacent plagioclases from Mount St Helens and 50 from Shiveluch for H_2O, major elements and trace elements using ion- and electron-microprobes (see Methods and Table 1).

Before applying any geothermometer or geobarometer, it is

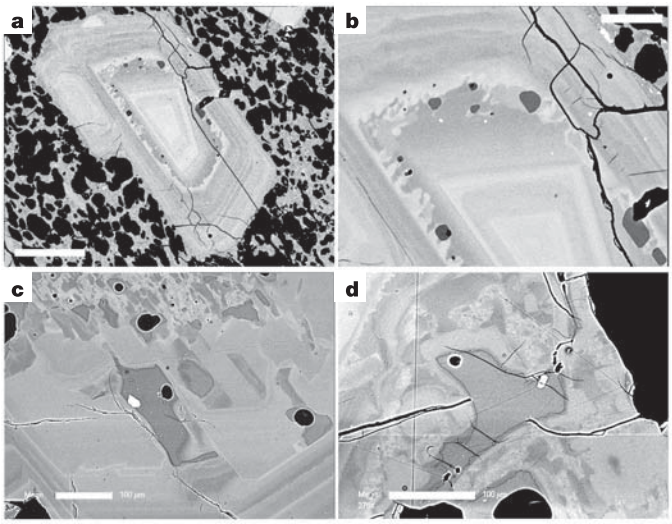

Figure 1 | Back-scattered electron micrographs of plagioclase-hosted melt inclusions from Mount St Helens. Variations in grey-scale in plagioclase denote compositional zoning from An-poor (dark) to An-rich (bright). The dark grey patches within plagioclase are melt inclusions; darker shades of grey denote higher dissolved H_2O. Black denotes cracks or gas bubbles. **a**, Melt inclusions preserved within a single resorption zone; sample was erupted on 7 August 1980. Note increase in An (lighter) on the rimward side of the resorption zone. **b**, Detail of **a**, showing presence of tiny vapour bubbles (black) in some inclusions. **c**, Melt inclusions within spongy plagioclase core; sample was erupted on 27 December 1980. Melt inclusions are surrounded by plagioclase, which itself crystallized from melt inclusions, eventually creating a chequerboard pattern of plagioclase pseudomorphs. Note oscillatory zoning in the phenocryst rim, in which wavy resorption horizons are overgrown by more An-rich plagioclase. Large inclusion in centre of the image contains tiny daughter microlites (white) of oxides and pyroxene, which also occur in the groundmass of this sample. **d**, Late-stage in-growth of plagioclase into melt inclusion; sample was erupted on 16 October 1980. As in **c**, note patchy texture produced by in-fill of the melt inclusion network. Small embayments of plagioclase into the melt inclusion, such as those just above the scale bar, are of the type used for plagioclase–melt thermometry. Scale bars 100 μm (**a**, **c**, **d**) and 25 μm (**b**).

[1]Department of Earth Sciences, University of Bristol, Wills Memorial Building, Bristol BS8 1RJ, UK. [2]Department of Geological Sciences, University of Oregon, Eugene, Oregon 97403-1272, USA.

imperative to ensure that it affords adequate accuracy and precision. In the case of converting H_2O in melt inclusions to the partial pressure of H_2O (p_{H_2O}), robust solubility models are available[6]. To determine crystallinity, we used ion-microprobe analyses of the trace elements Rb and Zr, which have bulk solid–melt partition coefficients <0.05. Crystallinity is then calculated relative to the average Rb or Zr content of the whole rock, which varies little between eruptions at each volcano. In the case of plagioclase–melt thermometry, we evaluated a recent thermometer[7] against a set of 145 plagioclase–melt pairs from published experiments[8–16] not used in the original calibration. These data involve hydrous rhyolitic melt at temperatures of 750–995 °C and total pressures (P_{tot}) of 15–313 MPa. The thermometer gives an absolute average deviation of ± 19 °C for this data set, which is an estimate of its accuracy. The precision of the calculated p_{H_2O} and temperature, based on propagation of analytical uncertainties, is ± 7 MPa and ± 10 °C, respectively. The p_{H_2O} can be roughly equated to P_{tot} (and hence to depth of crystallization), because the partial pressures of other dissolved volatile species (for example, CO_2, SO_2, H_2S, Cl and F) in these melt inclusions are relatively low[5]. For example, a small subset of bubble-free melt inclusions at Mount St Helens was measured for CO_2, again by ion-probe. The maximum CO_2 measured is 400 p.p.m. at 6 wt% H_2O, consistent with an additional partial pressure of CO_2 of $\sim$60 MPa; lower CO_2 contents of melt inclusions with <6 wt% H_2O makes the pressure correction less.

Calculated crystallinities, p_{H_2O} and temperatures for both volcanoes (Fig. 2) show a clear increase in crystallinity and temperature with decreasing p_{H_2O}. At Mount St Helens, the explosively erupted, microlite-free plinian magma of 18 May 1980 consistently records the highest p_{H_2O}, in keeping with rapid extraction of these magmas from a sub-volcanic reservoir 7 km or more below the surface[17]. All subsequent eruptions, in addition to pre-plinian samples derived from the shallow cryptodome, show a wide spectrum of p_{H_2O} and temperature consistent with slower ascent and less explosive eruption of magmas stored pre-eruptively over a wide depth range[17]. The increase in crystallinity (Fig. 2a, d) is an expected consequence of the increase in liquidus temperature with decreasing p_{H_2O} for H_2O-saturated liquids[18]. The increase in temperature (Fig. 2b, e), by up to 100 °C, is at first surprising, given that it accompanies an increase in crystallinity of up to 40 wt%. For the case of crystal-free, H_2O-saturated rhyolite melt undergoing isenthalpic ascent—a reasonable scenario for slowly-ascending samples—thermodynamic calculations suggest temperature increases of the order 25 °C for a 200 MPa pressure drop[4]. The rather greater temperature increase that we observe (Fig. 2a, d) indicates that the additional contribution of latent heat to the thermal budget is significant. Using data for plagioclase crystallization from anhydrous melts, Couch *et al.*[19] calculate a temperature rise of 2.3 °C per 1% of plagioclase crystallization. A similar calculation for crystallization of plagioclase + orthopyroxene + magnetite in the proportions observed at Shiveluch yields 3.2 °C per 1% crystallized. These values are entirely consistent with our data (Fig. 2). We note that at Mount St Helens the pressure–temperature trajectory crosses the amphibole-out boundary at around 120 MPa. Only melt inclusions from the plinian white pumice of 18 May 1980 lie entirely within the amphibole stability field, consistent with the absence of amphibole breakdown rims in these samples[20]. All other samples show a mixture of pressures and temperatures within and without the amphibole stability field, consistent with variable extents of amphibole reaction rim development in these more slowly ascending, less explosive magmas[20].

Independent support for the observed temperature rise comes from thermometry of touching Fe-Ti oxides, which are present in all eruptions studied, as phenocrysts, groundmass microlites, and inclusions in other phenocrysts. At each volcano, the temperature spread recorded by the oxides (Fig. 2c, f) closely matches that from plagioclase–melt thermometry of melt inclusions (Fig. 2a, d). Oxide

Table 1 | Samples studied

Sample number	Description	Date erupted	Alias
Mount St Helens*			
SH10†	Dense juvenile material from phreatic explosion	10 April 1980	
USNM 115379-34	Cryptodome magma in lateral blast deposit	18 May 1980	34
SH80D	Cryptodome magma in lateral blast deposit	18 May 1980	
C85-310	Pale grey (microlite-bearing) pumice‡		
KC518PFB	Microlite-free white pumice from pyroclastic flow	18 May 1980	PLZ, KCPL, May
May25†	Airfall pumice	25 May 1980	
KC612PF	Pumice from pyroclastic flow	12 June 1980	Jun
KC722U	Pumice from pyroclastic flow	22 July 1980	Jul
KC807B	Pumice from pyroclastic flow	7 August 1980	Aug
SHKB23§	Dense pumice in levee of 10/80 pyroclastic flow	7 August 1980	
USNM 115418-60-2	Dome fragment	16 October 1980	
USNM 115418-60	Dome fragment	16 October 1980	60
USNM 115418-42	Pumice	16 October 1980	
USNM 115418-61	Dome	16 October 1980	
USNM 115427-1	Pumice	27 December 1980	
USNM 115427-4	Dome	27 December 1980	
USNM 115465	Dome	18 June 1981	
KC681	Dome	18 June 1981	
USNM 115773-18	Dome	19 March 1982	
USNM 115773-3	Pumice	19 March 1982	
Shiveluch‖			
SHIV01/#1	Dome fragment	May 2001	
SHIV01/#2	Pumice	May 2001	
SHIV01/#3	Dome fragment	July 2001	
SHIV01/#4	Pumice	May 2001	
Shv202002	Dome fragment	July 2002	
Shv202003	Pumice	May 2001	

*USNM samples come from the Smithsonian Institution; where the same samples are designated with an alias in ref. 5 this is also given. All samples, except KC518PFB, contain microlite crystals in the groundmass.
†Source: Cascades Volcano Observatory.
‡Erupted during the initial basal pyroclastic flow (phase I) of the plinian eruption [32]. Likely remnant of cryptodome or conduit magmas.
§Sample location UTM 10562602E 5117871N.
‖Samples described in ref. 31.

inclusions in phenocrysts provide the most reliable estimate of conditions at the onset of magma ascent from the deep-seated magma reservoir (that is, ~870 °C at Mount St Helens and ~850 °C at Shiveluch). Oxide phenocryst pairs and groundmass microlites extend the temperature spread to higher values. As oxides chemically re-equilibrate to changes in temperature on a timescale of several days[21], the observed spread is consistent with partial re-equilibration of these oxides during decompression crystallization. This suggests that microlite-rich lava domes, which typically crystallize at shallow levels, will show higher equilibration temperatures than explosively erupted, microlite-poor magma of the same composition. These findings are in contrast to interpretations of spreads in oxide temperature data observed at other volcanoes, which include heating by new pulses of hotter, more-mafic magma just before eruption[21,22], or thermal stratification within the subvolcanic reservoir[23].

The rise in temperature during decompression crystallization can also be calculated thermodynamically for any hydrous andesite magma, provided that the variation in crystallinity with pressure and temperature is known. We have performed calculations for a generic H_2O-saturated silicic andesite (Fig. 3a), similar in composition to Mount St Helens and Mount Pinatubo magmas, ascending from 300 MPa with an initial (crystal-free) temperature of 880 °C and latent heat release of 2.3 °C per 1% crystallized. We consider both linear and nonlinear (polynomial) variations in crystal fraction (X) between solidus and liquidus. At each pressure, we solve the heat balance between crystallization and latent heat release to determine the equilibrium temperature, ignoring the heat of vapour exsolution or adiabatic expansion, which would make a small reduction to the calculated temperatures[4]. The calculated increases in temperature (Fig. 3b) and crystallinity (Fig. 3c) during decompression are similar for the linear and polynomial cases, and closely match the increases shown in Fig. 2. Amphibole breakdown starts at approximately 150 MPa (Fig. 3b).

Our results demonstrate that temperature increase caused by latent heat release is likely in any hydrous magma that decompresses sufficiently slowly to permit crystallisation, and a phenomenon that has important implications for the textures and physical properties of hydrous silicic magmas. For example, calculated low-pressure melt viscosities[24] are reduced by a factor of 5–10 compared to the

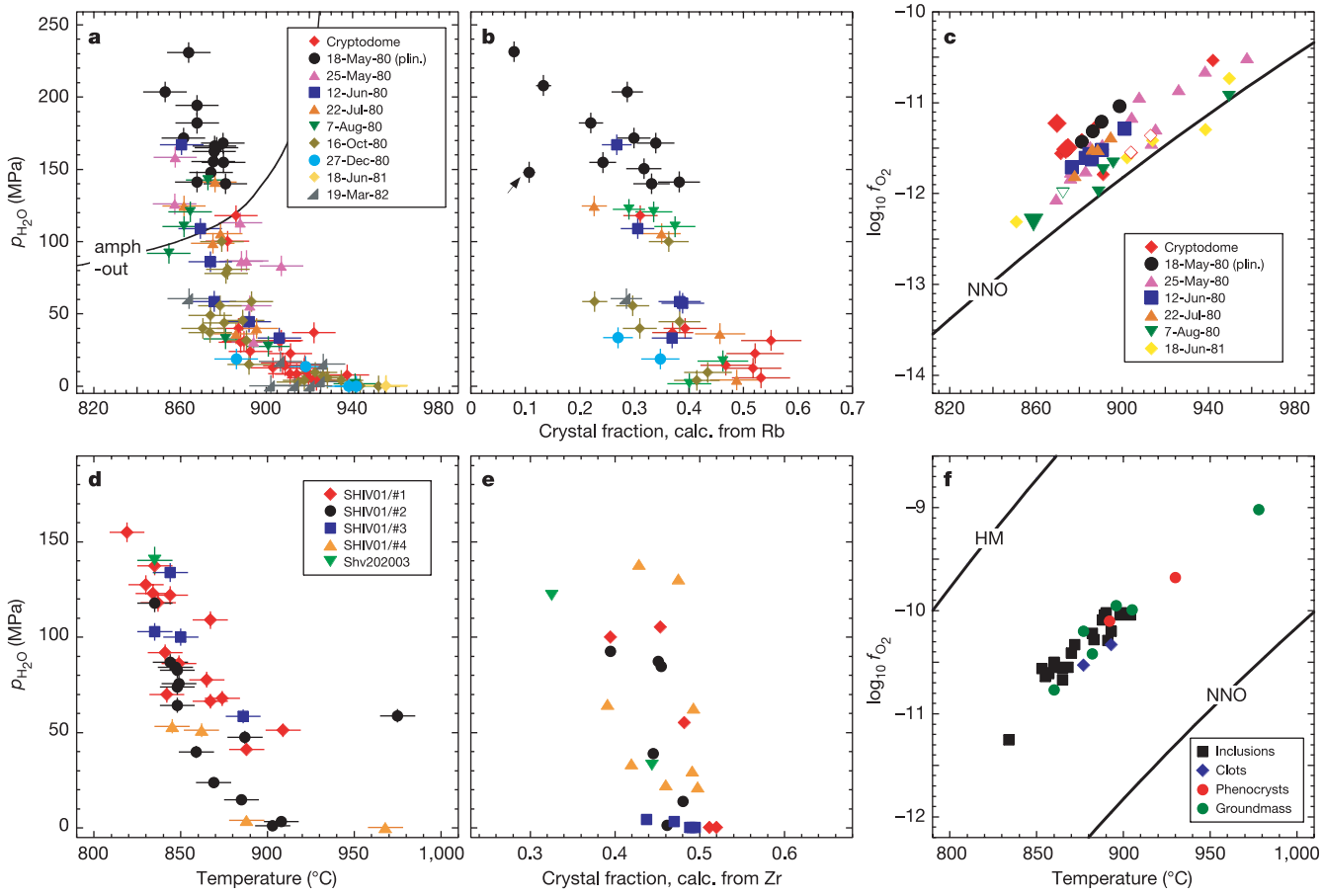

Figure 2 | Variation in magmatic variables. **a**–**c**, Beneath Mount St Helens; **d**–**f**, beneath Shiveluch. Data are taken from Supplementary Data Tables 1 and 2. Panels **a** and **d** show calculated p_{H_2O} (from measured H_2O) and temperature (from plagioclase–melt thermometry) in plagioclase-hosted melt inclusions. Data are distinguished on the basis of eruption age (**a**) or sample number (**b**). In **a**, 'Cryptodome' includes pre-18 May 1980 juvenile material, the lateral blast deposit and early microlite-bearing plinian sample C85-310[32]. Error bars are ±1 s.d. precision, as described in the text. The amphibole-out ('amph-out') curve in **a** is taken from ref. 20. Panels **b** and **e** show calculated variation in crystallinity as a function of p_{H_2O}. At Mount St Helens, crystallinity is calculated relative to the average whole-rock Rb content of 14 1980–86 dacites (30.8 ± 1.9 p.p.m.); at Shiveluch, we used the average whole-rock Zr of 112 ± 4 p.p.m. (ref. 31). Most of the scatter in **b** and **e** results from using a constant whole-rock trace element content for the crystallinity calculations, when in reality there will be small variations between different magma batches. This is especially true for a single melt inclusion from Mount St Helens, shown with an arrow in **b**, which has anomalous concentrations of all trace elements and appears to represent an exotic melt component. Panels **c** and **f** show the calculated equilibration temperature and oxygen fugacity (f_{O_2}) for touching Fe-Ti oxide pairs. The nickel–nickel oxide (NNO) and magnetite–haematite (HM) oxygen buffers are shown for reference. In **c**, inclusions in silicate phenocrysts (large filled symbols), phenocryst oxides (filled symbols), and groundmass microlites (open symbols) are distinguished on the basis of eruption date; in **f**, they are distinguished on the basis of texture, including crystal-rich 'clots'.

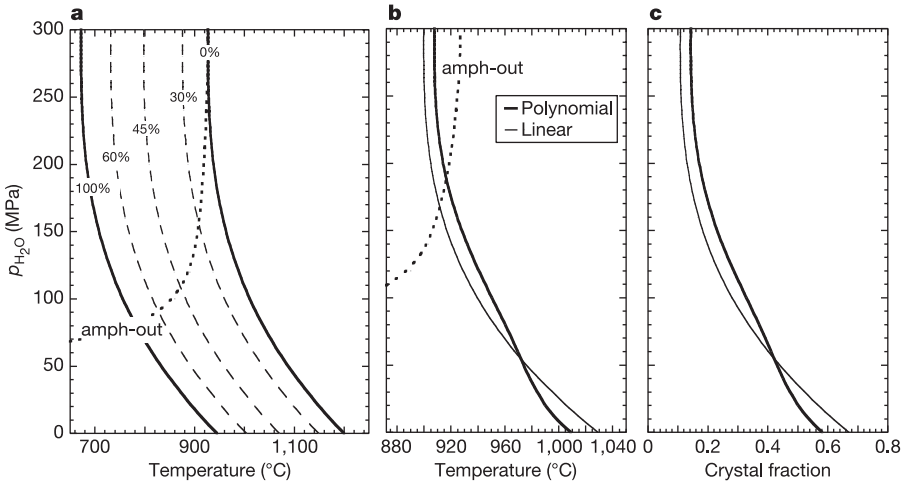

Figure 3 | Modelled variation in magmatic parameters during decompression of a generic H_2O-saturated silicic andesite. This material is similar in composition to Mount St Helens and Mount Pinatubo magmas. **a**, Phase diagram. Mount St Helens liquidus and haplogranite solidus parameterized from ref. 18. Crystal fraction (X, expressed as %) contours are based on a polynomial parameterization of 220 MPa H_2O-saturated experimental data on Mount Pinatubo[16]:

$$X = 2.757\left(\frac{T_L - T}{T_L - T_S}\right)^3 - 3.922\left(\frac{T_L - T}{T_L - T_S}\right)^2 + 2.165\left(\frac{T_L - T}{T_L - T_S}\right) \quad (1)$$

where T is temperature, T_L is the liquidus and T_S is the solidus at the pressure of interest. The amphibole-out (amph-out) curve is from ref. 20. **b**, Temperature based on linear variation of crystal fraction between solidus and liquidus (thin curve) and polynomial variation (equation (1), thick curve). **c**, Crystal fraction based on linear (thin curve) and polynomial (thick curve) variations. Calculations are based on an arbitrary initial temperature (crystal-free) at 300 MPa of 880 °C, which is slightly higher than that at either Mount St Helens or Shiveluch.

isothermal case, which serves to offset the increase in viscosity that results from degassing and crystallization. Such changes in melt viscosity may affect the kinetics of crystal and bubble formation and the ease of gas migration out of magma conduits, thereby influencing both the rate and style of eruptive activity. The textural consequences of exothermic crystallization are equally far-reaching. For example, heating will lead to reverse-zoned rims on phenocrysts of plagioclase, Fe-Ti oxides and pyroxenes, which might otherwise be attributed to a heating event by hotter, more-mafic magma just before eruption[21,22,25].

Heating may also bear on oscillatory zoning in plagioclase phenocrysts[26] because of the opposing effects of decompression and heating on equilibrium liquidus plagioclase compositions, which serve, respectively, to decrease and increase anorthite (An) content. At Mount St Helens, we calculate that decompression decreases An by ~0.5 mol% per 1 MPa pressure drop, while latent heat release increases An by ~3 mol% for each per cent crystallized. The complex interplay between the two effects will result in a regime where crystals both grow in response to decompression and resorb due to heating by adjacent batches of crystallizing magma. For an individual crystal, the result will be a saw-tooth pattern characteristic of normal-oscillatory zoning[26], in which a short, normally-zoned step due to decompression crystallization is truncated by a resorption horizon and then overgrown by slightly higher-An plagioclase (Fig. 1a–c) as the sample becomes heated. A detailed quantitative evaluation of this proposal is beyond the scope of this paper. However, if our interpretation of oscillatory zoning is correct, then there is considerable scope for using the amplitude and frequency of oscillations in plagioclase to quantify magma ascent rates through the sub-volcanic system. Our results demonstrate the importance of considering latent heat release in the textural interpretation of magmatic phenocrysts and in models of sub-volcanic magma movement and eruption dynamics.

METHODS

Analytical methods. Melt inclusions were analysed for their major elements by a Cameca SX100 wavelength-dispersive electron-microprobe with a 2–4 nA, 15 kV defocused beam (≥10 μm diameter) and reduced counting times for Na to reduce alkali loss during irradiation[27]. Oxide crystals were also analysed by electron-microprobe using a focused 10 nA, 20 kV beam. For oxide thermometry, only magnetite and ilmenite grains in direct contact with each other, or included in the same phenocryst, were analysed in order to sample the variability in magmatic temperatures within an individual sample. This is not possible with the conventional approach of using average analyses for thermometry. All analyses in our study meet the Mg-Mn equilibrium criterion of ref. 28. Oxide formulae were recalculated according to ref. 29; and temperature and oxygen fugacity were calculated using the method of ref. 30.

H_2O and light-element isotope (up to ^{47}Ti) contents of melt inclusions were analysed on a Cameca IMS4f ion-microprobe, using the method of ref. 5. Spot diameter at the sample surface was typically 8 μm for a 2 nA primary beam. A subset of the inclusions was analysed for heavy trace-element isotopes (^{47}Ti to ^{238}U) by ion-microprobe, in a separate analytical session from H_2O and light elements to reduce magnet hysteresis. All trace elements were calibrated against NIST SRM610 glass; ^{30}Si, as determined by electron-microprobe analysis of the same spot, was used as the internal standard for all analyses. Analysis of secondary standards indicates that accuracy is within 10–15% relative for all elements analysed. Precision is always <5% relative, based on counting statistics. In this study, a requirement for acceptance of any melt inclusion analysis is that measurements of Ti from electron-probe, light-element ion-microprobe routine and heavy-element ion-microprobe routine agree to within ±8% relative, and that the analytical total lies between 98.2 and 101.5 wt%. Melt inclusions that showed chemical or textural evidence for syneruptive loss of H_2O (ref. 5), without concomitant crystallization, were excluded from this study. Plagioclase ingrowths into, or adjacent to, melt inclusions were analysed by energy-dispersive techniques on a Hitachi S-3500N scanning electron microscope calibrated against plagioclase standards of variable An content. Reproducibility is within ±2.5 mol% An.

Melt inclusion analyses for Mount St Helens and Shiveluch are given in Supplementary Tables 1a and 1b, respectively; oxide analyses in Supplementary Tables 2a and 2b.

Received 15 March; accepted 17 July 2006.

1. Cashman, K. V. in *The State of the Planet: Frontiers and Challenges in Geophysics* (eds Sparks, R. S. J. & Hawkesworth, C. J.) 109–124 (AGU Monograph 150, American Geophysical Union, Washington DC, 2004).
2. Melnik, O. & Sparks, R. S. J. Non-linear dynamics of lava dome extrusion. *Nature* **402**, 37–41 (1999).
3. Melnik, O. & Sparks, R. S. J. Controls on conduit magma flow dynamics during lava dome building eruptions. *J. Geophys. Res.* **110**, doi:10.1029/2004JB003183 (2005).

4. Mastin, L. G. & Ghiorso, M. S. Adiabatic temperature changes of magma-gas mixtures during ascent and eruption. *Contrib. Mineral. Petrol.* **141,** 307–321 (2001).
5. Blundy, J. & Cashman, K. Rapid decompression-driven crystallisation recorded by melt inclusions from Mount St. Helens volcano. *Geology* **33,** 793–796 (2005).
6. Newman, S. & Lowenstern, J. B. VolatileCalc: a silicate melt–H_2O–CO_2 solution model written in Visual Basic for excel. *Comput. Geosci* **28,** 597–604 (2002).
7. Putirka, K. Igneous thermometers and barometers based on plagioclase + liquid equilibria: tests of some existing models and new calibrations. *Am. Mineral.* **90,** 336–346 (2005).
8. Costa, F., Scaillet, B. & Pichavant, M. Petrological and experimental constraints in the pre-eruption conditions of Holocene dacite from Volcán San Pedro (36°S, Chilean Andes) and the importance of sulphur in silicic subduction-related magmas. *J. Petrol.* **45,** 855–881 (2004).
9. Couch, S., Harford, C. L., Sparks, R. S. J. & Carroll, M. R. Experimental constraints on the conditions of formation of highly calcic plagioclase microlites at the Soufrière Hills volcano, Montserrat. *J. Petrol.* **44,** 1455–1475 (2003).
10. Hammer, J. E., Rutherford, M. J. & Hildreth, W. Magma storage prior to the 1912 eruption at Novarupta, Alaska. *Contrib. Mineral. Petrol.* **144,** 144–162 (2002).
11. Holtz, F., Sato, H., Lewis, J., Behrens, H. & Nakada, S. Experimental petrology of the 1991–1995 Unzen dacite, Japan. Part I: phase relations, phase compositions and pre-eruptive conditions. *J. Petrol.* **46,** 319–337 (2005).
12. Klimm, K., Holtz, F., Johannes, W. & King, P. L. Fractionation of metaluminous A-type granites: an experimental study of the Wangrah Suite, Lachlan Fold Belt, Australia. *Precambr. Res.* **124,** 327–341 (2003).
13. Larsen, J. F. Experimental study of plagioclase rim growth around anorthite seed crystals in rhyodacite melt. *Am. Mineral.* **90,** 417–427 (2005).
14. Martel, C. *et al.* Effects of fO_2 and H_2O on andesite phase relations between 2 and 4 kbar. *J. Geophys. Res.* **104,** 29453–29470 (1999).
15. Martel, C. & Schmidt, B. C. Decompression experiments as an insight into ascent rates of silicic magmas. *Contrib. Mineral. Petrol.* **144,** 397–415 (2003).
16. Scaillet, B. & Evans, B. W. The 15 June 1991 eruption of Mount Pinatubo. I. Phase equilibria and pre-eruption P-T-fO_2-fH_2O conditions of the dacite magma. *J. Petrol.* **40,** 381–411 (1999).
17. Scandone, R. & Malone, S. D. Magma supply, magma discharge and readjustment of the feeding system of Mount St. Helens during 1980. *J. Volcanol. Geotherm. Res.* **23,** 239–262 (1985).
18. Blundy, J. & Cashman, K. Ascent-driven crystallisation of dacite magmas at Mount St. Helens, 1980–1986. *Contrib. Mineral. Petrol.* **140,** 631–650 (2001).
19. Couch, S., Harford, C. L., Sparks, R. S. J. & Carroll, M. R. Mineral disequilibrium in lavas explained by convective self-mixing in open magma chambers. *Nature* **411,** 1037–1039 (2001).
20. Rutherford, M. J. & Hill, P. M. Magma ascent rates from amphibole breakdown: An experimental study applied to the 1980–1986 Mount St. Helens eruption. *J. Geophys. Res.* **98,** 19667–19686 (1993).
21. Venezky, D. Y. & Rutherford, M. J. Petrology and Fe-Ti oxide reequilibration of the 1991 Mount Unzen mixed magma. *J. Volcanol. Geotherm. Res.* **89,** 213–230 (1999).
22. Devine, J. D., Rutherford, M. J., Norton, G. E. & Young, S. R. Magma storage region processes inferred from geochemistry of Fe-Ti oxides in andesitic magma, Soufriere Hills Volcano, Montserrat, WI. *J. Petrol.* **44,** 1375–1400 (2003).
23. Hildreth, W. Gradients in silicic magma chambers: implications for lithospheric magmatism. *J. Geophys. Res.* **86,** 10153–10192 (1981).
24. Hess, K. U. & Dingwell, D. B. Viscosities of leucogranite melts: a non-Arrhenian model. *Am. Mineral.* **81,** 1297–1300 (1996).
25. Bachman, O. & Dungan, M. A. Temperature-induced Al-zoning in hornblendes of the Fish Canyon magma, Colorado. *Am. Mineral.* **87,** 1062–1076 (2002).
26. Ginibre, C., Kronz, A. & Wörner, G. High-resolution quantitative imaging of plagioclase composition using accumulated backscattered electron images: new constraints on oscillatory zoning. *Contrib. Mineral. Petrol.* **142,** 436–448 (2002).
27. Humphreys, M. C. S., Kearns, S. L. & Blundy, J. D. SIMS investigation of electron-beam damage to hydrous, rhyolitic glasses: Implications for melt inclusion analysis. *Am. Mineral.* **91,** 667–679 (2006).
28. Bacon, C. R. & Hirschmann, M. M. Mg/Mn partitioning as a test for equilibrium between coexisting Fe-Ti oxides. *Am. Mineral.* **73,** 57–61 (1988).
29. Spencer, K. J. & Lindsley, D. H. A solution model for coexisting iron-titanium oxides. *Am. Mineral.* **66,** 1189–1201 (1981).
30. Andersen, D. J. & Lindsley, D. H. Internally consistent solution models for Fe-Mg-Mn-Ti oxides: Fe-Ti oxides. *Am. Mineral.* **73,** 714–726 (1988).
31. Dirksen, O. V. *et al.* The 2001–2004 dome-forming eruption of Shiveluch Volcano, Kamchatka: observation, petrological investigation and numerical modelling. *J. Volcanol. Geotherm. Res.* **155,** 201–226 (2006).
32. Criswell, C. W. Chronology and pyroclastic stratigraphy of the May 18, 1980 eruption of Mount St. Helens, Washington. *J. Geophys. Res.* **92,** 10237–10266 (1987).

Supplementary Information is linked to the online version of the paper at www.nature.com/nature.

Acknowledgements J.B. was supported by an NERC Senior Research Fellowship and M.H. by an NERC Studentship. Ion-microprobe analysis benefited greatly from the efforts of the IMF staff at Edinburgh University and from standard materials supplied by T. Sisson, P. King and R. Brooker. W. Melson and D. Pyle provided some Mount St Helens samples.

Author Contributions The authors contributed equally to this work.

Author Information Reprints and permissions information is available at www.nature.com/reprints. The authors declare no competing financial interests. Correspondence and requests for materials should be addressed to J.B. (Jon.Blundy@bris.ac.uk).